

Article

# Hydrogeochemical and Isotopic Constraints on the Pattern of a Deep Circulation Groundwater Flow System

Xiting Long <sup>1,2,3</sup>, Keneng Zhang <sup>1,2</sup>, Ruiqiang Yuan <sup>4,\*</sup>, Liang Zhang <sup>5</sup> and Zhenling Liu <sup>6</sup>

<sup>1</sup> Key Laboratory of Metallogenic Prediction of Nonferrous Metals and Geological Environment Monitoring Ministry of Education, School of Geoscience and Infophysics, Central South University, Changsha 410083, China; longxiting@csu.edu.cn (X.L.); ken@csu.edu.cn (K.Z.)

<sup>2</sup> Hunan Key Laboratory of Nonferrous Resources and Geological Hazards Exploration, Changsha 410083, China

<sup>3</sup> The 402 Team, The Bureau of Geology and Mineral Resources Exploration of Hunan, Changsha 410014, China

<sup>4</sup> School of Environment and Resource, Shanxi University, Taiyuan 030006, China

<sup>5</sup> Department of Biological Sciences, University of Windsor, 401 Sunset Avenue, Windsor, ON N9B 3P4, Canada; zhang.on.ca@gmail.com

<sup>6</sup> Well Testing Sub-Company, BHDC, Langfang 065007, China; liuzhenling@cnpc.com.cn

\* Correspondence: rquyan@sxu.edu.cn; Tel./Fax: +86-0351-7010600

Received: 8 December 2018; Accepted: 21 January 2019; Published: 28 January 2019



**Abstract:** Characterization of a deep circulation groundwater flow system is a big challenge, because the flow field and aqueous chemistry of deep circulation groundwater is significantly influenced by the geothermal reservoir. In this field study, we employed a geochemical approach to recognize a deep circulation groundwater pattern by combined the geochemistry analysis with isotopic measurements. The water samples were collected from the outlet of the Reshui River Basin which has a hot spring with a temperature of 88 °C. Experimental results reveal a fault-controlled deep circulation geothermal groundwater flow system. The weathering crust of the granitic mountains on the south of the basin collects precipitation infiltration, which is the recharge area of the deep circulation groundwater system. Water infiltrates from the land surface to a depth of about 3.8–4.3 km where the groundwater is heated up to around 170 °C in the geothermal reservoir. A regional active normal fault acts as a pathway of groundwater. The geothermal groundwater is then obstructed by a thrust fault and recharged by the hot spring, which is forced by the water pressure of convection derived from the 800 m altitude difference between the recharge and the discharge areas. Some part of groundwater flow within a geothermal reservoir is mixed with cold shallow groundwater. The isotopic fraction is positively correlated with the seasonal water table depth of shallow groundwater. Basic mineral dissolutions at thermoneutral conditions, hydrolysis with the aid of carbonic acid produced by the reaction of carbon dioxide with the water, and hydrothermal alteration in the geothermal reservoir add some extra chemical components into the geothermal water. The alkaline deep circulation groundwater is chemically featured by high contents of sodium, sulfate, chloride, fluorine, silicate, and some trace elements, such as lithium, strontium, cesium, and rubidium. Our results suggest that groundwater deep circulation convection exists in mountain regions where water-conducting fault and water-blocking fault combined properly. A significant elevation difference of topography is the other key.

**Keywords:** deep circulation groundwater; groundwater flow; geothermal water; faults; isotopes

## 1. Introduction

There is a continuous heat-flow from the Earth's interior to the surface. Away from tectonic plate boundaries, geothermal gradient is about 25–30 °C/km of depth near the surface in most of the world [1]. For deep circulation groundwater, downward flow lowers crustal temperatures, while upward flow tends to raise temperatures. Deep circulation groundwater as part of the hydrologic cycle influences the distribution of heat and, thereby, the temperature field in the Earth's crust [2]. Deep circulation groundwater flow systems need more attention.

Deep circulation groundwater flow systems are usually connected to geothermal system, especially in neotectonic and volcanic areas. Geological structures relating to geothermal activities, such as faults, usually complicate the flow and chemistry of deep circulation groundwater. Generally, a geothermal system is mainly fed by meteoric water infiltrating at different altitudes including rain water and snowmelt [3–5]. Mountain regions are usually the recharge area [6,7]. Flow and geochemistry of geothermal water are usually structurally controlled [4,8]. Fault zone permeability influences the spatial distribution and behavior of hydrothermal and geothermal systems at all scales. Areas of spatial interaction between two groups of faults are structurally ideal places for concentrated hydrothermal activity [9].

Geothermal waters from metamorphic, granite, and sedimentary regions exhibit varying hydrogeochemical features [10]. Variant types of geothermal waters can be formed, such as HCO<sub>3</sub>-Ca, HCO<sub>3</sub>-Na, SO<sub>4</sub>-Na (Ca), and Cl-SO<sub>4</sub>-Na type [10–12]. Enhanced water–rock interaction increases concentrations of major and trace elements in geothermal waters. It was reported that the sodium and chloride concentrations of geothermal fluid reach up to 16,963 mg/L and 68,256 mg/L in a volcanic geothermal system, respectively [13]. It is possible that the deeply sourced geothermal fluids cause degradation of water quality of the shallow groundwater and surface water [14]. In addition, the geothermal water might show an altered water isotopic composition by a stronger oxygen shift in the deeper reservoir [7]. Although geothermal water is chemically different with cold water of the same area in most cases, the similarity of geothermal and cold water in chemical and isotopic compositions also exists [3].

Mixing is a common process during the upward flow of geothermal water. Geothermal waters might be a mixture of magmatic water, stream, deep geothermal fluids, shallow geothermal fluids, and cold water from the surface [13,15–19]. Mixing is also a process that controls outlet temperatures and causes dilution of geothermal water [5]. At the same time, mixing blurs the information of the deep circulation groundwater.

Deep circulation groundwater flow systems are structurally and geochemically complex. Isotopic investigations combined with geothermal applications represent powerful tools for the exploration of deep circulation groundwater flow systems [6,7,12]. In this study, a deep circulation hydrothermal system was surveyed based on hydrogeochemical and isotopic constraints to elucidate the origin of the geothermal fluids and the source of solutes and to discern the mixing and the hydrogeochemical alteration. The main goal is to gain a conceptual model and mechanisms for the deep circulation groundwater flow system.

## 2. Study Area

### 2.1. Geographical Settings

The study area, the Reshui River Basin, located around E 113°54' and N 25°32' with subtropical monsoon humid climate in southeast China. The multi-year average precipitation is 1670 mm. About 50% of annual precipitation happens during April to August. The coldest month is January with an average temperature of 6.5 °C, while the warmest month is July with a mean temperature of 27.8 °C. The annual mean air temperature is about 16.7 °C. The landscape is mainly hills and mountains with small basins distributed. Elevation changes from 200 m to 1700 m. Forests cover more than 70% of

land surface. Many streams drain the area. The Shangyoujiang River has an annual mean flow of  $16 \text{ m}^3/\text{s}$  (Figure 1).

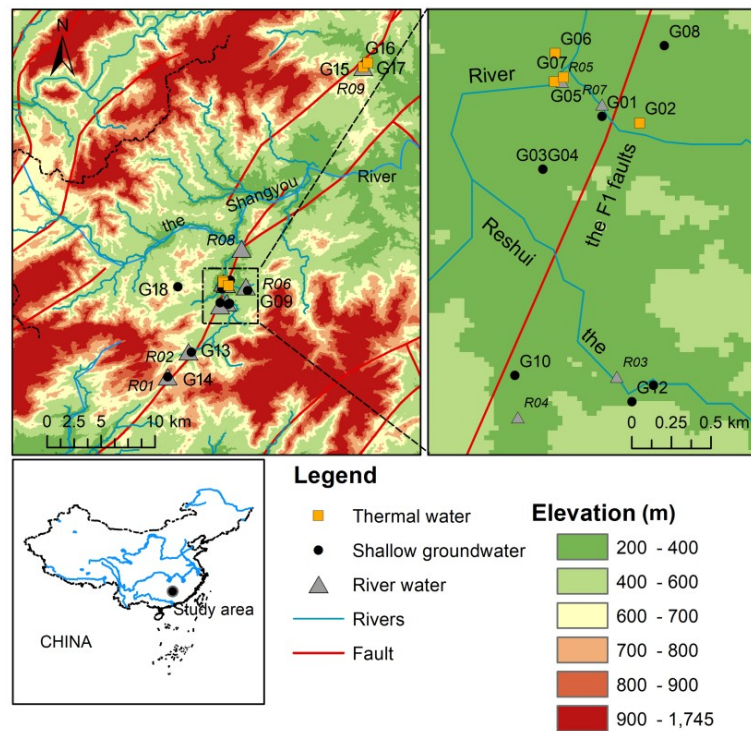


**Figure 1.** Elevation, rivers, main faults, and sampling sites in the study area.

## 2.2. Geological and Hydrogeological Settings

The study area is within the plate collision zone between the Cathaysian block and the Yangtze block. The exposing strata mainly include Sinian strata and Precambrian strata. Intrusive rocks are mainly monzonite granite formed during Triassic to Jurassic distributing on the east and south. There are four fault systems that dominated the geologic structure (Figure 2).

The F1 fault is an active about 200 km long fault system. Master faults strike NE and dip NW with an angle ranging  $78\text{--}87^\circ$ . The fault-throw is about several decameters. Many warm springs discharge waters controlled by the fracture system, which infers that the major fault of the system could penetrate deeply the crust. The F2 fault parallels to F1 located around 15 km on the southeast of the F1. The F2 is a NW dipping fracture system with an angle about  $50^\circ$ . The fault-throw changes from several meters to several decameters. The F3 is a SE dipping active normal fault with an angle  $70\text{--}85^\circ$ . The fracture zone is 7–12 m wide. The F4 is a NW trending thrust fault system with a maximum fault-throw about 20 m. The dipping angle of the F4 fault is around  $66^\circ$  towards SW.

The unconsolidated Quaternary alluvial sediments are distributed in the river valley. The sediment can be divided into two layers. The upper layer is sandy clay with a thick of 1–5 m. The second layer is gravels and sandy clay, which is 1–3 m thick. Mountains and hills are mainly outcrops of sandstone, slate, and granite (Figure 2). The thickness of weathering crusts ranges from 9 m to 24 m.

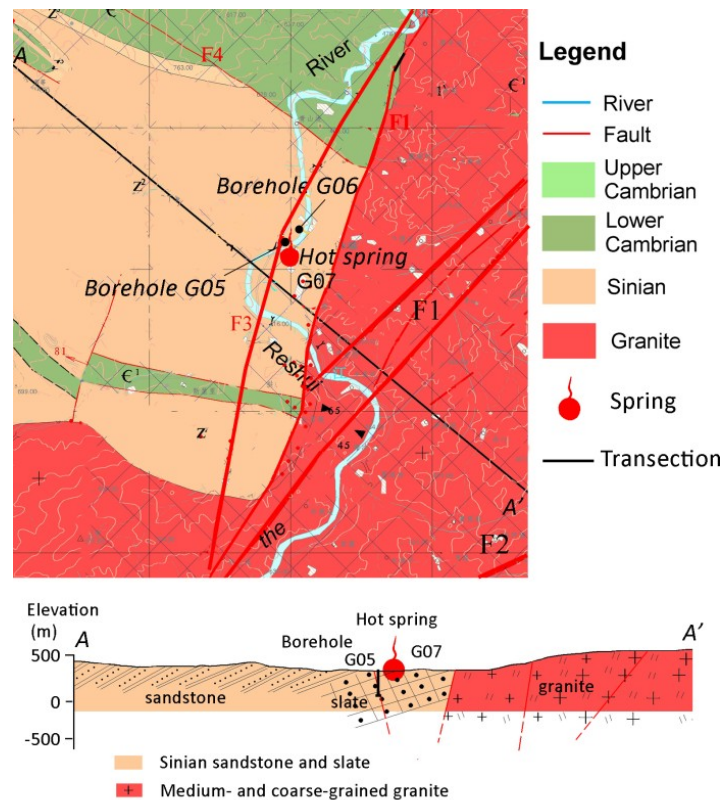


**Figure 2.** Geological sketch of the study area (revised from unpublished data).

There are three kinds of groundwater including: (1) pore water in unconsolidated sediments; (2) fissure water in weathering fracture and structural fracture of bedrocks outcrops; and (3) deep circulation groundwater. Groundwater occurred in Quaternary sediment exchanges with rivers seasonally and distributes in basins. The fissure water is recharged by precipitation flowing within fracture networks until discharged as spring or into Quaternary sediment on the base of slopes. The unconsolidated sediment and fracture networks of weathered crust are a connected system in which shallow groundwater flows. A part of the fissure water flows downwards into the deep through fault systems alimenting the deep circulation groundwater.

### 2.3. Thermal-Geological Features

The Reshui hot spring geothermal field has an area about 3 km<sup>2</sup>. The spring locates on the riverside of the Reshui River that is a tributary of the Shangyoujiang River. A vertical stratum of slate forms the river bed where the hot spring discharges. The temperature of the spring water is usually around 90 °C with a maximum of 98 °C. Several boreholes were drilled around the hot spring. The production of hot water is up to 2500 m<sup>3</sup>/d in total.

Boreholes with hot water (outlet temperature 84.6–92.2 °C) and the hot spring are distributed along the line trending 110–115°. Crustal derived granite locates on the east and the south of the hot spring. The geothermal field might be heated by magma activities and radioactive decay.

## 3. Method

Two field surveys were conducted on September 2016 and February 2017, respectively. Water samples of shallow groundwater, river water, and geothermal water were collected for major ions, trace elements,  $\delta D$ , and  $\delta^{18}O$  (Figure 1). Samples of G07, G15, G16, and G17 were collected from geothermal springs. Samples of G02, G05, and G06 were collected from boreholes reaching the deep fissure network. The depths of the boreholes are 500, 200, and 150 m, respectively. The other groundwater samples were collected from open wells. Some of the wells are artesian on rainy seasons

(summer). Before sampling, we measured water table depths and physicochemical parameters in situ (Horiba U-51 calibrated in advance), such as water temperature, pH, electrical conductivity (EC), oxidation-reduction potential (ORP). Water samples were collected in a 100 mL syringe and filtered immediately through 0.45  $\mu\text{m}$  cellulose-ester membranes into three 60 mL and one 100 mL high density polyethylene (HDPE) bottles, which were filled to overflowing and capped. The samples in the 100 mL bottles were used for titration of bicarbonate on the day of sampling. The samples for cation analysis were acidified immediately ( $\text{pH} = 2$ ).

Water samples were analyzed in the laboratory of the Institute of Geographic Sciences and Natural Resources Research, Chinese Academy of Sciences. The chemical compositions were characterized by ICP-OES (PerkinElmer, Optime 5300 DV, Waltham, MA, USA) for cations and Ion Chromatography (Shimadzu LC-10ADvp) for anions. The trace elements (Al, Ag, As, Ba, Be, Bi, Cd, Co, Cu, Cr, Cs, Fe, Ga, In, Li, Mn, Mo, Ni, Rb, Pb, Se, Sr, Sb, Tl, Ti, U, V, Zn) were analyzed by an inductively coupled plasma mass spectrometry (PerkinElmer, ICP-MS Elan DRC-e). Hydrogen and oxygen stable isotopic compositions of the water samples were analyzed by the isotope ratio mass spectrometer (Finnigan MAT-253, Silicon Valley, CA, USA) using the TC/EA (high-temperature conversion/elemental analyzer) method. The  $\delta^{18}\text{O}$  and  $\delta\text{D}$  values were reported as per mill (‰) deviations from the international standard V-SMOW (Vienna Standard Mean Ocean Water). The  $\delta^{18}\text{O}$  and  $\delta\text{D}$  measurements were reproducible to  $\pm 0.2\text{‰}$  and  $\pm 1\text{‰}$ , respectively.

## 4. Results

### 4.1. Deep Circulation Geothermal Groundwater (TW) Features

Upward flow of the deep circulation groundwater usually carries heat of crust from the depth showing a high temperature. The water temperature is around 88 °C in the thermal spring (G07), which is located close to the F3 fault and the F1 fault. Long-term stress conditions would favor continuous fluid flow through vertical high-flux conduits in the faults [9]. While the borehole (G05) drilled into the F3 fault fractured zone with a depth about 200 m discovered the geothermal water directly with a water temperature of 93 °C. Given heat loss of water during ascending, the geothermal water temperature could be higher than 93 °C at the depth. The difference between G05 and G07 was induced by longer residence time and more heat loss of the geothermal water in fractures compared to the geothermal water in the borehole. The other geothermal water from springs or boreholes had water temperatures lower than 60 °C. It is suggested that the mixing of deep circulation geothermal groundwater with shallow cold groundwater in the subsurface. Based on the G05 and G07, the deep circulation geothermal water shows a pH value around 8.7 and an EC value about 340  $\mu\text{S}/\text{cm}$ . Both were significantly higher than other water samples (Table 1 and Figure 3). The concentration of  $\text{CO}_2$  degassing usually results in the geothermal water pH increase [19].  $Eh$  (estimated by measured ORP values) of the geothermal water changes from 173 mV to 271 mV between September and February, which significantly lower than other water samples.

The hydrogeochemical type (Figure 4) of the deep circulation geothermal groundwater is  $\text{HCO}_3\text{-SO}_4\text{-Na}$  (September rainy season) or  $\text{HCO}_3\text{-SO}_4\text{-Na}$  (February dry season). The water isotopic composition is  $\delta^{18}\text{O} -7.2\text{‰}$  and  $\delta\text{D} -45\text{‰}$  in average (Table 1). The concentrations of  $\text{SiO}_2$  and  $\text{F}^-$  are about 150 mg/L and 10 mg/L, respectively. Specially, the trace elements, for example Li (370  $\mu\text{g}/\text{L}$ ), Rb (38  $\mu\text{g}/\text{L}$ ), Cs (36  $\mu\text{g}/\text{L}$ ), Mo (23  $\mu\text{g}/\text{L}$ ), As (15  $\mu\text{g}/\text{L}$ ), and Ga (3  $\mu\text{g}/\text{L}$ ) are significantly higher in the deep circulation geothermal groundwater than those in other water samples. Moreover, there is no obviously seasonal variance in hydrogeochemical features of the deep circulation geothermal groundwater.

Table 1. Results of hydrochemical measurements.

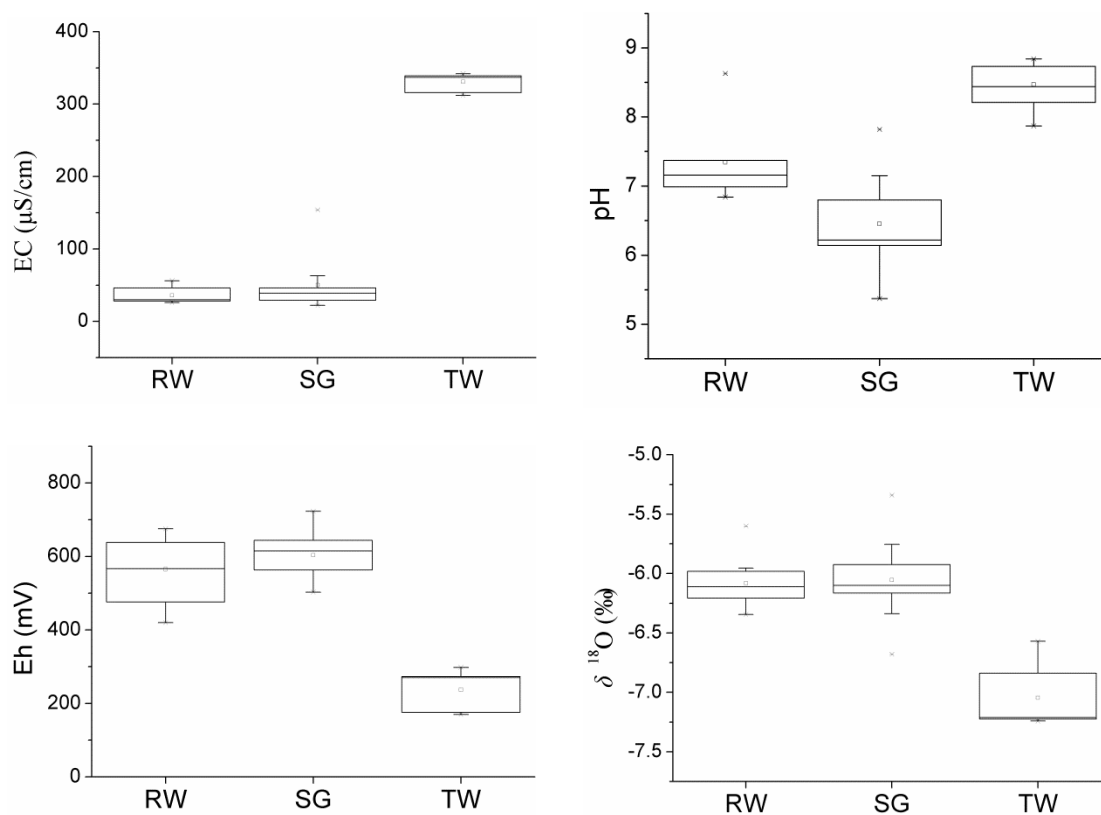
Sites	Sampling Date	Type	pH	EC (us/cm)	Eh (mV)	$\delta^{18}\text{O}$ (‰)	$\delta\text{D}$ (‰)	$\text{Ca}^{2+}$ (mg/L)	$\text{Mg}^{2+}$ (mg/L)	$\text{Na}^{+}$ (mg/L)	$\text{K}^{+}$ (mg/L)	$\text{HCO}_3^{-}$ (mg/L)	$\text{SO}_4^{2-}$ (mg/L)	$\text{Cl}^{-}$ (mg/L)	$\text{NO}_3^{-}$ (mg/L)	$\text{F}^{-}$ (mg/L)	$\text{SiO}_2$ (mg/L)	Fe ( $\mu\text{g/L}$ )	Al ( $\mu\text{g/L}$ )
G01	201702	SG	6.4	115	627	-6.1	-36	9.3	1.9	8.3	3.6	56.0	7.1	5.0	12.3	-	29.9	2.7	11.8
G02	201609	TW	6.8	144	475	-6.0	-36	17.7	2.3	8.2	2.8	99.5	2.0	1.6	1.0	0.2	46.05	2.8	60.8
G02	201702	TW	6.98	159	625	-5.6	-33	17.3	2.3	9.6	2.8	103.5	2.7	4.4	7.1	-	43.9	2.1	26.4
G03	201702	SG	6.14	46	676	-6.1	-36	4.0	1.1	3.5	2.0	27.0	1.3	2.5	7.1	-	18.3	1.6	4.4
G04	201702	SG	6.51	154	723	-6.1	-34	15.4	3.9	12.4	2.8	61.0	16.4	8.3	4.1	-	19.8	1.3	26.7
G05	201609	TW	8.84	342	176	-7.2	-46	4.9	0.1	53.2	3.2	126.0	32.9	2.4	6.1	10.1	150.2	23.0	47.6
G05	201702	TW	8.73	339	270	-7.2	-44	4.5	0.1	60.8	3.0	112.7	37.6	3.6	0.1	-	144.3	31.9	3.5
G06	201609	TW	7.87	312	298	-6.6	-41	14.5	3.8	39.5	4.2	130.1	23.5	6.4	4.1	6.8	126.5	3.6	42.2
G06	201702	TW	8.21	316	558	-6.8	-41	12.3	2.0	50.4	3.2	118.1	34.3	4.0	0.1	-	127.0	14.3	15.5
G07	201609	TW	8.44	339	170	-7.2	-46	4.8	0.1	52.0	2.9	123.5	33.6	4.6	0.9	10.2	153.5	40.8	14.4
G07	201702	TW	8.73	337	273	-7.2	-44	4.0	0.0	62.3	2.9	112.7	37.5	3.6	0.1	-	149.4	26.9	1.2
G08	201702	SG	6.22	63	664	-5.8	-34	3.5	1.4	7.0	1.7	40.5	3.1	1.8	4.6	-	33.3	3.0	-
G09	201609	SG	5.74	43	578	-5.9	-36	16.9	0.8	5.6	1.0	88.0	1.4	2.2	1.6	0.2	33.96	0.8	58.8
G09	201702	SG	6.22	43	644	-6.1	-37	3.1	0.6	6.3	0.8	35.0	0.8	0.4	0.8	-	30.4	1.9	-
G10	201609	SG	6.2	33	533	-6.1	-36	4.5	1.4	2.4	1.8	38.0	1.1	1.5	1.0	0.1	20.89	6.3	19.7
G10	201702	SG	7.15	33	631	-6.3	-37	2.7	1.4	2.6	1.3	30.0	0.8	0.2	1.3	-	21.3	17.8	11.8
G11	201609	SG	5.37	41	563	-5.3	-33	23.2	0.7	4.4	1.4	100.0	1.1	2.0	1.0	0.1	26.81	3.7	78.6
G11	201702	SG	7.82	39	615	-6.0	-35	8.0	0.5	4.7	1.2	47.0	1.4	1.3	5.2	-	26.9	5.1	5.0
G12	201702	SG	6.88	29	622	-6.2	-35	3.2	0.2	4.2	1.2	20.0	1.2	0.3	2.0	-	26.7	6.2	-
G13	201609	SG	6.68	37	503	-6.3	-38	9.9	0.5	3.3	2.0	40.0	2.0	2.0	7.6	0.1	27.87	30.1	52.4
G13	201702	SG	7.09	26	592	-5.8	-33	2.8	0.1	4.6	1.4	19.5	1.7	0.6	1.1	-	27.4	32.5	-
G14	201702	SG	6.16	22	580	-6.0	-34	1.8	0.1	2.7	1.7	14.0	0.8	0.4	0.6	-	22.5	2.7	-
G15	201702	TW	6.85	196	265	-6.7	-40	9.9	1.3	27.6	5.5	112.2	7.8	1.2	1.3	-	57.1	4.4	4.9
G16	201702	TW	7.66	259	520	-7.1	-43	7.7	0.7	50.2	2.5	137.1	10.5	2.2	1.4	-	68.1	4.8	2.2
G17	201702	TW	7.76	368	263	-7.6	-48	9.3	0.2	72.1	2.8	189.8	12.9	3.5	1.2	-	85.2	4.8	3.8
G18	201609	SG	6.8	56	503	-6.7	-39	11.9	1.3	3.2	1.2	63.0	2.1	1.9	2.1	0.3	24.78	6.3	39.5
R01	201702	RW	6.96	28	567	-6.0	-35	1.2	0.1	3.6	1.5	12.2	1.0	0.5	2.1	-	23.5	13.5	-
R02	201609	RW	7.03	26	476	-6.1	-35	2.4	0.2	2.6	1.0	16.0	1.9	2.2	2.0	0.2	19.47	58.1	34.7
R02	201702	RW	7.26	27	638	-6.1	-34	7.6	0.2	3.1	0.9	23.0	2.7	0.4	1.8	-	19.0	58.1	15.4
R03	201609	RW	7.16	30	517	-5.6	-35	3.6	0.3	2.9	1.2	10.0	0.1	5.2	3.4	0.6	19.59	20.7	42.9
R03	201702	RW	7.37	29	629	-6.4	-35	2.0	0.2	3.0	1.0	9.8	1.7	0.6	2.2	-	17.7	4.8	-
R04	201609	RW	6.84	34	448	-6.1	-36	9.8	1.1	2.7	1.5	38.8	0.1	2.3	0.1	0.1	19.29	19.6	65.5
R04	201702	RW	8.05	36	613	-6.2	-36	2.1	1.0	2.8	1.2	19.5	1.6	0.6	1.7	-	18.9	16.6	14.1
R05	201609	RW	7.12	46	420	-6.3	-37	4.4	0.7	3.2	1.6	22.0	5.0	3.5	0.5	0.2	19.73	8.1	19.3
R05	201702	RW	7.17	41	658	-6.1	-36	11.0	0.7	3.6	1.2	36.0	2.5	1.1	3.6	-	19.3	13.1	17.1
R06	201609	RW	7.31	26	476	-6.2	-37	2.0	0.2	2.9	1.2	11.0	2.5	5.1	1.8	0.6	21.2	13.7	18.3
R06	201702	RW	6.96	30	644	-6.0	-36	1.4	0.2	3.9	1.3	12.0	2.2	1.0	2.2	-	21.7	22.1	3.6
R07	201702	RW	6.99	47	625	-6.0	-34	3.4	0.6	4.5	1.7	17.8	2.4	1.4	3.5	-	21.6	6.3	6.7
R08	201702	RW	7.98	46	675	-6.0	-34	3.2	0.6	4.9	1.3	26.0	3.0	1.0	2.4	-	21.9	7.7	-
R09	201702	RW	8.63	56	527	-6.2	-36	3.6	1.0	6.0	1.8	31.2	2.1	1.0	2.5	-	26.3	9.6	5.0

**Table 2.** Calculated saturation indexes on September 2016.

Sites	Type	Talc	Chlorite	Chrysotile	Sepiolite	Willemite	Calcite	Aragonite	Dolomite	K-Mica	Quartz	Chalcedony	Goethite	Hematite	Fe(OH) <sub>3</sub> (a)	K-Feldspar	Kaolinite	Ca-Montmorill	Illite	Gibbsite
G05	TW	9.49	7.49	4.84	1.22	6.38	0.62	0.51	-0.2	-1.96	0.4	0.14	5.3	12.85	-2.52	-2.16	-	-5.68	-5.43	-2.92
G07	TW	7.5	5.2	2.6	0.03	3.38	0.44	0.33	-0.5	0.35	0.54	0.28	4.99	12.23	-2.75	-1.41	-2.13	-3.46	-3.6	-2.13
G06	TW	7.9	-	2.95	0.75	2.56	0.4	0.28	0.64	-	0.66	0.36	6.18	14.56	-1.24	-	-	-	-	-
G02	TW	-5.41	-	-9.98	-6.15	-2.11	-1.23	-1.37	-3	-	0.86	0.43	7.23	16.46	1.33	-	-	-	-	-
G09	SG	-14.12	-	-18.47	-11.8	-7.33	-2.41	-2.56	-5.85	-	0.79	0.35	6.42	14.82	0.66	-	-	-	-	-
G11	SG	-16.92	-	-21.06	-13.71	-7.16	-2.59	-2.74	-6.41	-	0.68	0.24	6.16	14.31	0.4	-	-	-	-	-
G10	SG	-10.9	-19.39	-14.78	-9.93	-2.8	-2.8	-2.94	-5.75	6.94	0.52	0.09	6.33	14.66	0.42	-1.24	4.43	2.78	0.76	1.28
G18	SG	-7.32	-13.84	-11.37	-7.45	-3.39	-1.6	-1.74	-3.82	7.56	0.61	0.18	7.07	16.14	1.22	-0.58	4.57	3.32	1.55	1.26
G13	SG	-9.01	-15.7	-13.15	-8.58	-2.66	-1.98	-2.12	-4.92	9.47	0.66	0.22	7.09	16.18	1.22	0.22	5.77	4.74	2.89	1.82
R02	RW	-8.33	-13.98	-12.13	-8.32	-1.85	-2.58	-2.72	-5.87	8.72	0.46	0.04	7.01	16.03	1.04	-0.36	5.21	3.88	2.18	1.73
R04	RW	-7.71	-13.5	-11.54	-7.74	-2.6	-1.84	-1.98	-4.29	8.27	0.51	0.07	7.34	16.68	1.95	-0.46	4.95	3.62	1.49	1.56
R03	RW	-6.99	-12.96	-10.79	-7.44	-1.04	-2.47	-2.61	-5.65	7.09	0.46	0.04	7.17	16.37	1.2	-0.76	3.98	2.52	1.01	1.11
R05	RW	-6.19	-12.15	-10	-6.88	-2.32	-2.09	-2.24	-4.61	6.45	0.47	0.04	6.87	15.75	0.9	-0.91	3.5	1.97	0.58	0.87
R06	RW	-6.81	-13.59	-1.84	-7.54	-1.69	-0.74	-2.76	-6.78	6.49	0.53	0.1	6.97	15.96	1.1	-0.73	3.51	2.04	0.62	0.81

**Table 3.** Calculated saturation indexes on February 2017.

Sites	Type	Talc	Chrysotile	Sepiolite	Calcite	Aragonite	Quartz	Chalcedony
G05	TW	9.12	4.46	0.91	0.52	0.42	0.39	0.14
G07	TW	7.72	2.65	1.24	0.41	0.29	0.83	0.49
G06	TW	-	-	-	0.42	0.31	0.52	0.24
G02	TW	-4.68	-9.23	-5.56	-1.08	-1.23	0.87	0.44
G15	TW	-4.22	-8.86	-5.89	-1.23	-1.36	0.79	0.39
G16	TW	-0.85	-5.73	-3.21	-0.58	-0.72	0.98	0.56
G17	TW	-0.39	-5.34	-3.39	-0.14	-0.27	0.92	0.54
G01	SG	-9.53	-13.79	-8.63	-2.24	-2.39	0.77	0.32
G03	SG	-12.64	-16.48	-10.75	-3.16	-3.3	0.57	0.12
G04	SG	-9.36	-	-8.29	-1.98	-2.13	0.68	0.21
G08	SG	-10.63	-14.97	-12.17	-2.94	-3.09	0.8	0.36
G09	SG	-12.46	-16.77	-10.37	-3.12	-3.27	0.84	0.38
G10	SG	-6.74	-10.77	-6.46	-2.36	-2.51	0.73	0.26
G11	SG	-3.38	-7.58	-6.95	-1	-1.16	0.79	0.32
G12	SG	-10.11	-14.31	-8.84	-2.68	-2.83	0.78	0.32
G13	SG	-10.23	-14.5	-8.69	-2.6	-2.76	0.86	0.38
G14	SG	-15.2	-19.22	-12.43	-3.74	-3.89	0.66	0.2
R01	RW	-10.66	-14.74	-9.25	-3.22	-3.37	0.72	0.26
R02	RW	-8.86	-12.8	-7.87	-1.94	-2.09	0.69	0.21
R03	RW	-8.34	-12.22	-7.51	-2.75	-2.91	0.66	0.19
R04	RW	-2.1	-6.03	-5.85	-1.77	-1.92	0.69	0.22
R05	RW	-7.82	-11.78	-9.68	-1.68	-1.83	0.7	0.22
R06	RW	-10.44	-14.5	-8.88	-3.23	-3.38	0.75	0.28
R07	RW	-8.32	-12.32	-7.71	-2.59	-2.74	0.68	0.22
R08	RW	-2.72	-6.76	-6.4	-1.51	-1.66	0.72	0.26
R09	RW	2.4	-1.74	-3.17	-0.72	-0.88	0.75	0.29

**Figure 3.** Hydrochemical comparison of geothermal water (TW) to river water (RW) and shallow groundwater (SG).

#### 4.2. Shallow Groundwater (SG) Features

The circulation of deep geothermal water is deeply different with the shallow groundwater. The water table depth of the shallow groundwater is less than 0.5 m. Mean pH value is 6.1 in September and 6.7 in February for the shallow groundwater, while the average Eh values were 540 mV and 640 mV, respectively. EC value rarely changes in the shallow groundwater with a mean value about 40  $\mu\text{S}/\text{cm}$ . Compared with the deep circulation groundwater, the shallow groundwater is weakly mineralized, oxidized, neutral, or slightly acidic.

The hydrogeochemical type of the shallow groundwater is  $\text{HCO}_3\text{-Ca}$  (September rainy season) or  $\text{HCO}_3\text{-Na}\cdot\text{Ca}$  (February dry season). The mean water isotopic compositions are  $\delta^{18}\text{O} -6.1\text{‰}$  and  $\delta\text{D} -36\text{‰}$ . The concentrations of  $\text{SiO}_2$  and  $\text{F}^-$  are about 26 mg/L and 0.2 mg/L (Table 1), respectively. The trace element concentrations are lower than the deep circulation geothermal water.

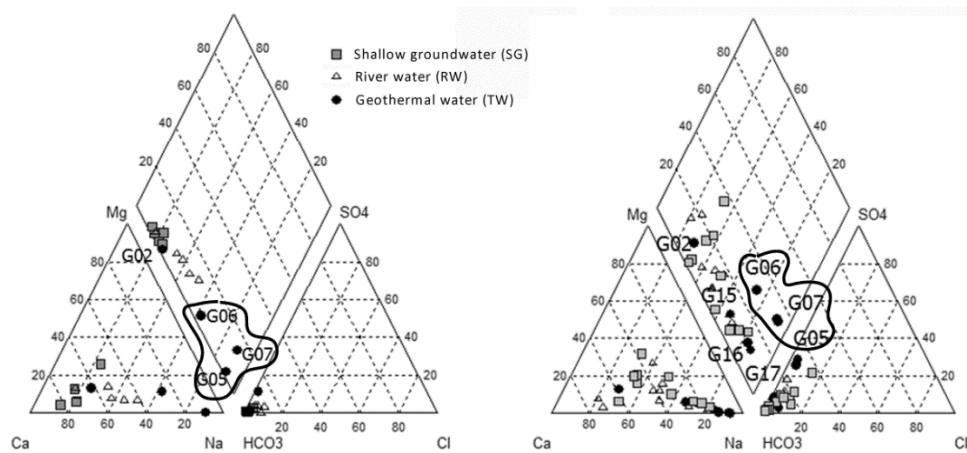
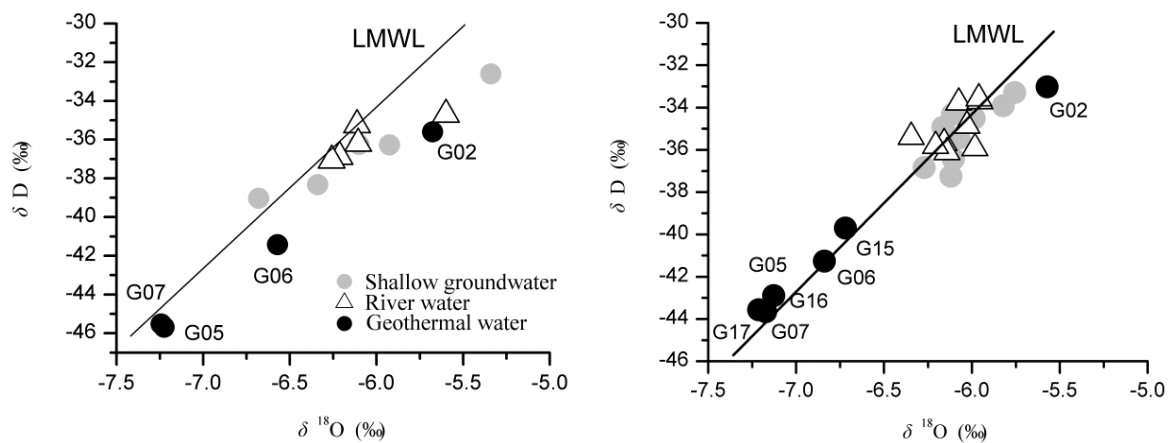


Figure 4. Piper plots in September rainy season (left) and February dry season (right).

#### 4.3. River Water (RW) Features

The river water originates from the spring and outflowing shallow groundwater, which can be inferred from the water isotopes data (Figure 5). As a result, river water shows similar hydrogeochemical features to the shallow groundwater. Mean pH values are 7.2 in September and 7.5 in February for the river water, while the average Eh values are 470 mV and 620 mV, respectively. EC value rarely changes for the river water with a mean value about 38  $\mu\text{S}/\text{cm}$ . The hydrogeochemical type of the river water is  $\text{HCO}_3\text{-Ca}\cdot\text{Na}$  (September rainy season) or  $\text{HCO}_3\text{-Na}\cdot\text{Ca}$  (February dry season). The mean water isotopic compositions are  $\delta^{18}\text{O} -6.1\text{‰}$  and  $\delta\text{D} -36\text{‰}$ . The concentrations of  $\text{SiO}_2$  and  $\text{F}^-$  are about 20 mg/L and 0.3 mg/L, respectively. The trace element concentrations are generally lower than the deep circulation geothermal water. The river water is also weakly mineralized, oxidized, and neutral.



**Figure 5.** Isotopic compositions in different waters. The left is derived from the survey in September. The right is based on the result of February. The isotopic composition of the deep circulation geothermal water (G05 and G07) obviously depletes in heavy water isotopes indicating a different water source with other waters. The shallow groundwater is subject to evaporation in September due to very small depth of water table (<0.5 m), which tends to make an isotopic signal of the water locating below the local meteorological water line (LMWL).

## 5. Discussion

### 5.1. Mixing of Deep Circulation Groundwater (TW) with Shallow Groundwater (SG)

Mixing with shallow cool groundwater usually happens during the ascending of deep circulation groundwater. Mixing ratios should be considered accurately before assessing the deep circulation groundwater flow system based on hydrogeochemical and isotopic data. The thermal water from the borehole (G05) is withdrawn directly from the fracture zone of the F3 fault with a water temperature of 93 °C that is the highest among all water samples. The geothermal water (G05) and the geothermal spring (G07) are chemically equivalent featured by high contents of sodium, sulfate, chloride, fluorine, silicate, and some trace elements—such as lithium, strontium, cesium and rubidium. Moreover, the distinct physicochemical features exist between the geothermal water in G05 and G07 and the other water samples (Figure 3 and Table 1). According to the Figure 6 which identifies two end-members and the mixing line, geothermal groundwater from G05 and G07 are considered as the deep circulation water occurring in the geothermal reservoir without mixing with shallow cool groundwater (15 °C in February and 23 °C in September in average).

The shallow groundwater flows from east, west, and south to the Reshui geothermal field area following the topographic gradient with very shallow water table depth (within 0.5 m). In September, the end of rainy season, shallow groundwater receives significant recharge from precipitation. As a result, a part of wells even became artesian. In February, the period of low flow, water table depth falls with cease of the artesian wells. The seasonal change of water table depth strongly suggests a seasonal groundwater flow enhanced during rainy seasons. The seasonality of precipitation also caused differences in hydro-geochemistry of the shallow groundwater. As shown in Figure 6, the shallow groundwater has an identical hydrogeochemistry after a rainy season (September). However, a part of shallow groundwater gains more  $\text{Na}^+$  and  $\text{SO}_4^{2-}$  during a dry season (February). Based on a two end-member mixing mechanism, a mixing line connects the deep circulation groundwater and the shallow groundwater (Figure 6). Therefore, we confirmed that (1) the geothermal water G06 is the mixture of the deep circulation geothermal groundwater and the local shallow groundwater; and (2) the geothermal water G15, G16, and G17 belong to another geothermal system (Figure 6).

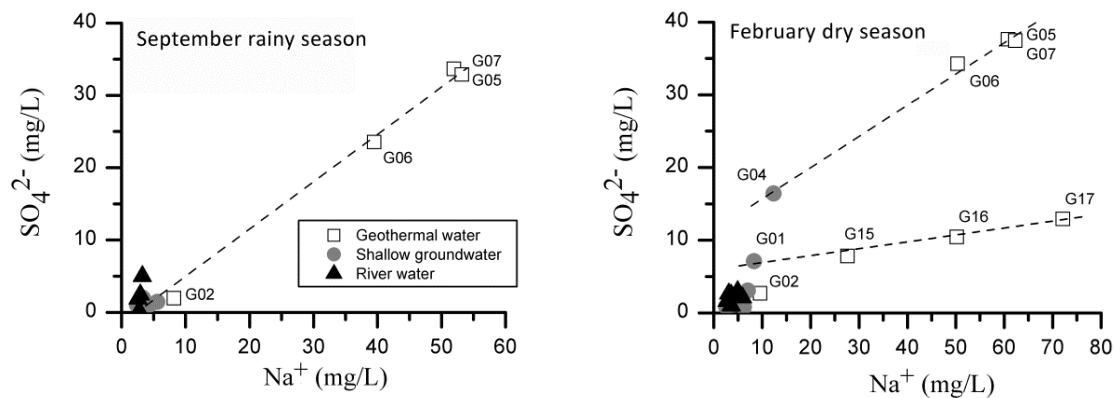


**Figure 6.** Plots of  $\text{Na}^+$  versus  $\text{SO}_4^{2-}$  reveal the relationship between end-members. The left is derived from the survey in September. The right is based on the result of February.

Geothermal water of G02, G05, G06, and G07 belongs to the Reshui geothermal field, while the geothermal water of G15, G16, and G17 comes from another geothermal system named here the Nuanshui geothermal field. The two deep circulation geothermal water systems can also be verified by distinct hydrogeochemical features. The geothermal water of the Nuanshui geothermal field (G17) shows a little higher EC (370  $\mu\text{S}/\text{cm}$ ) and lower pH (7.8) than water in the Reshui system. The hydrogeochemical type of G17 is  $\text{HCO}_3\text{-Na}$  with obviously lower content of  $\text{SO}_4^{2-}$  compared to the G05 and G07 (Figure 6). Moreover, the concentrations of trace elements such as Li (417  $\mu\text{g}/\text{L}$ ), Sr (137  $\mu\text{g}/\text{L}$ ), Cs (101  $\mu\text{g}/\text{L}$ ), and As (22  $\mu\text{g}/\text{L}$ ) in G17 are higher than that of G05 and G07 (Figure 7).

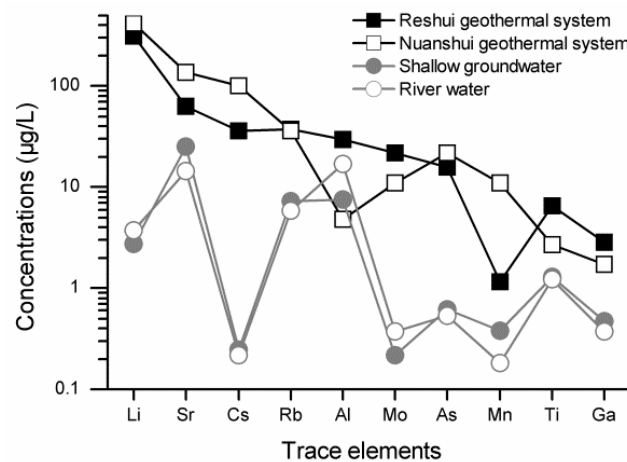


**Figure 7.** Trace elements concentrations in deep geothermal water (the mean of G05 and G07 represents the Reshui geothermal system, while G17 stands for the Nuanshui geothermal system), shallow groundwater (samples mean) and river water (samples mean). The other thermal water had obviously lower contents than G05, G07, and G17.

Based on the two end-member mixing method and tracer concentrations of  $\text{Na}^+$  and  $\text{SO}_4^{2-}$ , the average mixing ratio of the deep thermal water is 71% in September (the rainy season) and 81% in February (the dry season) for G06. The mixing ratio decreases obviously during the rainy season, which is consistent with the enhanced shallow groundwater flow in rainy seasons. The borehole of G06 has a depth about 150 m where the upward deep geothermal water mixes with the shallow groundwater flow. When pumping, the water table depth drops down about 50 m. Once pumping ceases, the water table depth recovers quickly closing to the ground surface. The mixing ratio of the deep circulation geothermal groundwater only slightly changes from 5% to 6% for G02. The depth of borehole G02 is over 500 m drilled into thick diorite discovering thermal water with a temperature

around 88 °C at the depth of 150 m. After the cease of pumping, shallow groundwater mixes into the borehole and dominated in the borehole tube.

### 5.2. Water Source of Deep Circulation Groundwater

The local meteorological water line (LMWL) is characterized as  $\delta D = 8.42 \delta^{18}O + 16.28$  based on water isotopes in precipitation of Guilin (1983–1998) [20] that are close to the study area with similar climate and geographical conditions. All samples of the study area are plotted around the LMWL indicating local precipitation origin of water (Figure 5). The deep circulation geothermal water, G05, G07, and G17 show the most depleted isotopic compositions. The shallow groundwater and the river water have similar isotopic compositions with an identical average isotopic composition ( $\delta^{18}O -6.1\text{‰}$  and  $\delta D -36\text{‰}$  on September,  $\delta^{18}O -6.0\text{‰}$  and  $\delta D -35\text{‰}$  on February). In addition, the shallow groundwater is significantly influenced by evaporation on September showing a more enriched isotopic composition.

The geothermal water of G06, G15, and G16 are distributed along the LMWL between G05, G07, and G17 and the average of shallow groundwater (Figure 5). It is the result of mixing of the ascending deep circulation geothermal water with the shallow groundwater. It should be noticed that the Reshui geothermal groundwater system and the Nuanshui geothermal groundwater system cannot be separated by isotope data due to the same precipitation isotopic input. The geothermal water of G02 shows an obviously enriched isotopic composition. The borehole G02 discovers deep circulation geothermal groundwater. The highest water temperature was observed around 88 °C, when the borehole was pumped. However, the borehole has been sealed for near a year long before our sampling with no pump installed. The water table depth was about 24.6 m with an around 500 m long water column in the borehole tube. The depth of the aquifer is about 150 m. We collected water samples from about 50 m below the ground surface. According the geochemical features (Table 1, Figures 4–6), the river water and shallow groundwater should have mixed into the borehole. Water in the tube is hard to flow and ready to be evaporated (Figure 5). Evaporation of waters also hinders the distinguishing of mixtures based on geochemical data.

The distinct distributions of isotopic compositions suggest different water sources. Water source areas can be identified by water isotopic compositions in surface water, groundwater and precipitation. Globally, the stable isotope lapse rate (change in stable isotope composition with elevation, namely, the altitude effect in precipitation isotopes) was reported to be in the range  $-0.15$  and  $-0.5\text{‰}$  per 100 m altitude increase for  $\delta^{18}O$  [21]. Altitude is considered as the main geographic control on  $\delta^{18}O$  in precipitation in Southern China with a lapse rate about  $-0.20\text{‰}$  for every 100 m [22]. The average  $\delta^{18}O$  in shallow groundwater and rivers is  $-6.1\text{‰}$  with an elevation about 350 m in the lower part of the basin. At the same time, the mean value is  $-7.2\text{‰}$  in the deep circulation geothermal groundwater. However, the  $\delta^{18}O$  at the leeward slope of mountains is around  $0.5\text{‰}$  larger than that at the windward slope induced by continuous rain-out processes associated with orographic lifting at the windward side and sub-cloud evaporation at the leeward side [21]. The south China belongs to the eastern Asia monsoon region with rainy seasons controlled by south to north wet monsoon. It is suggested that the mean  $\delta^{18}O$  should be revised as around  $-7.7\text{‰}$  due to the leeward sampling positions. Therefore, the average recharge elevations are estimated about 1150 m for G05 and G07 of the Reshui geothermal system. The mean recharge elevation is close to the altitude of the halfway up to surrounding mountain tops, which suggested that the mixture of precipitation infiltration from different heights of mountains is the source of the deep circulation geothermal water. For the Reshui geothermal groundwater system, the water source area is located in the surrounding high mountains on the south.

### 5.3. Ion Origin and Phase Equilibrium of Minerals in Deep Circulation Groundwater

Simple solution and hydrolysis contributed to mineralization of the water. According to saturation indexes of minerals calculated by PHREEQCI [23], shallow groundwater and river water are supersaturated with respect to hematite, K-mica, goethite, kaolinite, Ca-montmorillonite, illite, gibbsite,

quartz, and chalcedony (Tables 2 and 3), which are contained in widely distributed granite, slate, and quartz sandstone. These minerals contribute to constituents in water of the study area. Granite and slate covering most part of the watershed are usually hard to be weathered. However, carbonic acid formed by the reaction of carbon dioxide with the water takes apart in and promotes weathering progresses to derive mineral constituents such as metals and silica from granites. It is supported by a high percent of anionic milliequivalent of bicarbonate (average 82%) and the low pH value (average 6.4) in the shallow groundwater that means high activity of the hydrogen ion induced by the reaction of carbon dioxide with the water. Thus carbon dioxide takes an important role in the weathering of rock-forming minerals.

Compared with shallow groundwater and river water, the deep circulation geothermal water (G05 and G07) in the Reshui geothermal groundwater system is also supersaturated with respect to some altered minerals, such as talc, chrysotile, chlorite, and sepiolite (Tables 2 and 3), which is related with geothermal activities in depth supporting the deep circulation pattern [13]. Moreover, the deep circulation geothermal water shows distinct major ion chemistry. First, the content of sodium and sulfate are about ten times higher than that in shallow groundwater and river water. Second, the concentration of carbonate is around three times higher than that of shallow groundwater and river water. Third, there was no nitrate in the deep circulation geothermal water considering the rational measurement precision. The most widespread source of sodium is the weathering of feldspars in the study area. The deep circulation geothermal water in the Reshui geothermal system originated from the surrounding mountains on the south where feldspars are one of the common rock-forming minerals. Moreover, the weathering of feldspars would be promoted under geothermal condition with fresh replenishing of geothermal fluid. In hydrothermal environments, *S* is common and usually presents as sulfides. The sulfides would be oxidized to sulfates once exposed to the atmosphere or oxygenated. Therefore, substantial sodium and sulfate enter into the deep circulation geothermal water in the deep geothermal reservoir. However, the main source of nitrate in the water seems to be biologic activities in near-surface zones, forest litter, and the soil. During the deep circulation of the geothermal water, the nitrate could be consumed up by chemical and biochemical processes under an oxygen-deficient situation. That is the reason why nitrate is only observed in the shallow groundwater and the river water. Differences in saturation indexes of minerals and major ion chemistry suggest the different flow paths of the shallow groundwater and the deep circulation groundwater.

The deep circulation geothermal water (G05 and G07) also showed high contents of silicate and fluorine. The average concentrations of the silicate and fluorine are 150 mg/L and 10 mg/L in the geothermal water, respectively, which is consistent with a low temperature and large circulation depth geothermal water. At the same time, the concentrations are only 23 mg/L and 0.2 mg/L in the shallow groundwater and river water. Plagioclase, followed by K-feldspar and the ferromagnesian silicate minerals, are the major sources of dissolved silica in the groundwater. Large silica concentrations suggest that hydrolysis of primary silicates is a major process in the thermal water system. The very high saturation indexes (higher than 5) of hematite, K-mica, kaolinite, talc, and so on suggest the formation of secondary minerals, which is an indicator of a slowly flowing system.

The significant seasonal variation of phase equilibria of minerals is recorded for the shallow groundwater and river water that are supersaturated with respect to hematite, K-mica, goethite, kaolinite, Ca-montmorillonite, illite, gibbsite, quartz, and chalcedony in September and only quartz and chalcedony in February (Tables 2 and 3). Hematite, K-mica, and other clay minerals are chemical weathering productions of igneous rock by hydrolysis. Granite mountains are located on the south of the study area with a developed crust of weathering. In September, air temperature is high. Shallow groundwater ascends and even becomes artesian due to plenty rainfall during the rainy seasons when the weathering crust is flushed. Chemical weathering of the crust is intensive. As a result, the shallow groundwater and the river water are supersaturated with respect to hematite and clay minerals. In February, air temperature is low. Shallow groundwater descends and artesian springs disappear, because rainfall is infrequent. The crust would be exposed to dry air. The chemical

weathering of the crust is greatly weakened. Chemical weathering changed seasonally following the seasonality of precipitation, which is presented by the seasonal variation of saturated minerals in the shallow groundwater and river water.

#### 5.4. Circulation Depth and Passageway

Due to mixing with shallow cool groundwater, the geothermal water of G06 and G02 do not represent the true geothermal reservoir fluid and hence geothermal reservoir temperature estimated using geothermometers would deviate true value [3,17]. Geothermal water from G05 and G07 does not mix with the shallow cool groundwater. The geochemistry could represent the original result of the water-mineral equilibrium between the geothermal reservoir fluid and the host rocks in the geothermal reservoir. Chemical geothermometers give the last equilibration temperature for the reservoir. Many geothermometry techniques have been developed to predict reservoir temperatures in geothermal systems. All of these techniques are based on the assumption that temperature dependent water-mineral equilibrium is attained in the reservoir. The Na-K-Mg triangular diagram technology of Giggenbach [24] shows the geothermal water samples of G05 and G07 are located on the partial equilibrium zone (Figure 8). According to the saturation index of quartz (Tables 2 and 3), the ascending geothermal water is still saturated with silica. Therefore, geothermometers based on Na-K and SiO<sub>2</sub> can be used. However, the rates at which different species react vary, with silica adjusting faster than cations like Na<sup>+</sup> and K<sup>+</sup>. Moreover, concentrations of SiO<sub>2</sub> in G05 and G07 are around 150 mg/L that is so high that SiO<sub>2</sub> loss (aggregation and precipitation) during sample storage has to be considered. The average reservoir temperature is estimated at 177 °C by the Na-K geothermometers [24,25], 173 °C [26], and 161 °C [27]. Therefore, the temperature of the geothermal reservoir is estimated as 170 °C, which is the average of results from above methods. When considering 13% SiO<sub>2</sub> loss during sample storage, the same result of reservoir temperature is reached by the SiO<sub>2</sub> geothermometer (no steam loss) based on quartz solubility [28]. Our result suggested that a cation geothermometer, such as Na-K, typically has a longer ‘memory’ during the storage than SiO<sub>2</sub> geothermometer when the thermal water has high SiO<sub>2</sub> concentrations.

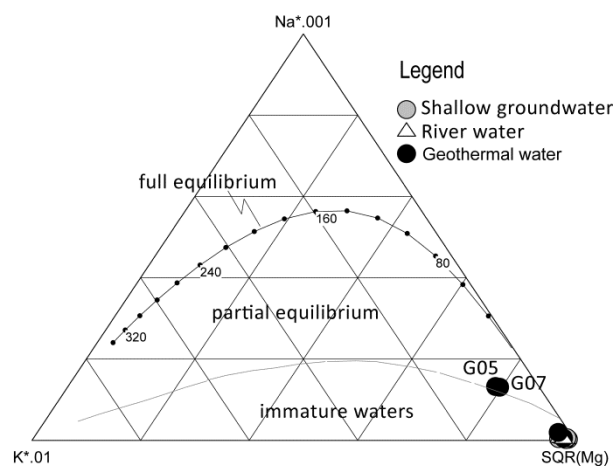


Figure 8. Ternary giggenbach's diagram (samples data in mg/L).

The equilibration temperature and the geothermal gradient of the region could offer a reliable estimate of the depth of geothermal reservoirs using the following formula [7]

$$D = (T - T_0)/K \times 1000 \quad (1)$$

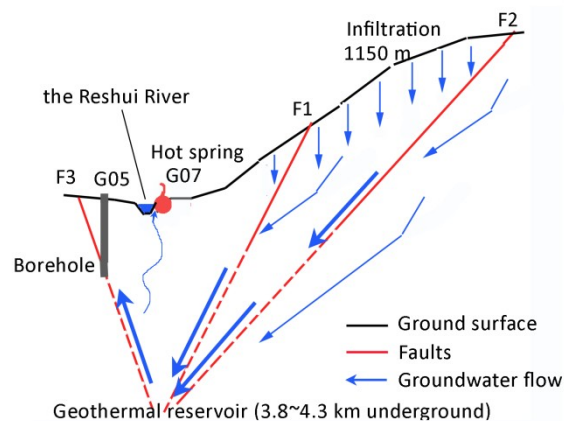
where  $D$  is the reservoir depth (m);  $T$  is the reservoir temperature (°C);  $T_0$  is the temperature of constant temperature zone (16.7 °C);  $K$  is geothermal gradient (°C/km). In South China, the average geothermal gradient is 24.1 °C/km, and the average heat flow is 64.2 mW/m<sup>2</sup> [29]. However, land

plate boundaries and the active zones of the deep faults are coincident with anomalies of high heat flow values and high geothermal gradient. The Reshui geothermal field is within the plate collision zone with the measured heat flow values ranging 60–100 mW/m<sup>2</sup> that is obviously higher than the average. Referencing to the result of Yuan et al. [29], geothermal gradients of 35 °C/km and 40 °C/km are employed in this study. The depth of the geothermal reservoir is estimated ranging between 3.8–4.3 km using Equation (1), which indicates the circulation depth of the geothermal water.

The deep circulation geothermal water is recharged on the southern mountains. However, the geothermal reservoir is located 10 km northward away and 3.8–4.3 km in depth. The NE trending fault systems of F1, F2, and F3 penetrate the granite and connect the recharge area and the geothermal reservoir offering the passageway for the deep circulation groundwater.

### 5.5. Conceptual Model of the Deep Circulation Groundwater

Based on the above discussion, the pattern of the deep circulation geothermal water in the Reshui low-temperature geothermal field is reconstructed (Figure 9). The deep circulation geothermal water originates from precipitation infiltration in the southern mountains with an average elevation about 1150 m. The infiltrating water flows downward in the fracture network of the weathering crust, and then a part of the groundwater converges into the F1 (the dipping angle 78–87°) and F2 (the dipping angle 50°) fault fracture zones (trending NNE–SSW). Groundwater in the fault fracture zones moves downward and northward under the pressure of water from the recharge highlands. The deep circulation water is heated by deep heat sources to a temperature around 170 °C at a depth of 3.8–4.3 km. Simple solution and hydrolysis contribute to mineralization of the deep circulation water that is also supersaturated with respect to some altered minerals—such as talc, chrysotile, chlorite, and sepiolite—by hydrothermal alteration. Therefore, the hydrogeochemical features are distinct with the shallow groundwater. The alkaline deep geothermal water enriches in Na, F, Li, and other trace elements consistent with the granite reservoir nature [19]. The bicarbonate geothermal water with some sulfate and a little chloride is mainly heated by conduction partially by steam in the reservoir.



**Figure 9.** Sketch of the conceptual model of the geothermal groundwater flow system.

However, the deep circulation geothermal water encounters a 110° trending thrust fault F4 which hindered the movement of the deep circulation geothermal water. The deep circulation geothermal water subsequently flows upwards to approach the surface along the F3 fault fracture zone driving by high water pressure originating an elevation difference about 800 m between recharge and discharge areas of the deep circulation groundwater and reduced density after heating. A part of the ascending geothermal water directly discharges into the Reshui River valley forming the Reshui Spring (G07). The deep circulation geothermal water (G05) is derived from F3 fault. The other recharges into the overlying phreatic aquifer mixing with the local cool shallow groundwater (G06).

## 6. Conclusions

Deep circulation groundwater flow systems are usually connected to geothermal system, especially in neotectonic and volcanic areas. Based on hydrogeochemical and isotopic data, the deep circulation groundwater flow system was surveyed in the Reshui geothermal field where an 88 °C hot spring occurs. Precipitation, mostly falling in the highlands, is the water source of the deep circulation groundwater flow system. The weathering crust of the granite mountain on the south collects infiltration of precipitation, which is recognized as water source area of the deep circulation groundwater. The average recharge elevation is about 1150 m. A regional active normal fault system formed the passageway connecting the water source area on the surface and the deep geothermal reservoir. Groundwater from the surface circulates to a depth about 3.8–4.3 km where the water is heated up to around 170 °C by conduction and partially by steam from the geothermal reservoir. The ongoing geothermal water is obstructed by a thrust fault system. Then the geothermal water flows upwards and forms the hot spring forcing by the water pressure of convection derived from the 800 m elevation difference between the recharge (the south mountains) and discharge (the hot spring) areas. The geothermal water is equilibrium with hot rocks in the geothermal reservoir. A simple solution of minerals, hydrolysis with the aid of carbonic acid produced by the reaction of carbon dioxide with the water, and hydrothermal alteration in the geothermal reservoir contribute ions to the deep circulation geothermal water. The alkaline deep circulation geothermal water is chemically featured by high contents of sodium, sulfate, chloride, fluorine, silicate, and some trace elements—such as lithium, strontium, cesium, and rubidium—and by depleted water isotopic compositions. Although the hydrogeochemistry of deep circulation groundwater is greatly changed in the geothermal reservoir, the isotopic investigations combined with geothermal applications still represent powerful tools for the exploration of deep circulation groundwater flow system in a geothermal field.

Our results suggest that groundwater deep circulation convection exists in where water-conducting fault and water-blocking fault combined properly. A water-conducting fault with a bigger dipping angle would act as a passageway for deep circulation convection. Significant elevation difference in topography is the other key. Those conditions would be met in mountain areas in most cases. Groundwater would seldom circulate to a significant depth in plain regions, usually due to the thick and layered alluvial deposits.

**Author Contributions:** Conceptualization, R.Y. and K.Z.; Methodology, X.L.; Software, L.Z.; Validation, R.Y. and Z.L., K.Z. and L.Z.; Formal Analysis, R.Y.; Investigation, X.L. and R.Y.; Data Curation, X.L.; Writing-Original Draft Preparation, X.L. and R.Y.; Writing-Review & Editing, R.Y.

**Funding:** This research was funded by the National Natural Science Foundation of China grant number 41301033.

**Acknowledgments:** The authors thank the 402 team in the Bureau of Geology and Mineral Resources Exploration of Hunan for research support, especially Xinping Deng for field survey assistance and data sharing.

**Conflicts of Interest:** The authors declare no conflict of interest.

## References

1. Fridleifsson, I.B.; Bertani, R.; Huenges, E.; Lund, J.W.; Ragnarsson, A.; Rybach, L. The Possible Role and Contribution of Geothermal Energy to the Mitigation of Climate Change. In Proceedings of the IPCC Scoping Meeting on Renewable Energy Sources, Proceedings, Luebeck, Germany, 20–25 January 2008; pp. 59–80.
2. Kooi, H. Groundwater flow as a cooling agent of the continental lithosphere. *Nat. Geosci.* **2016**, *9*, 227. [[CrossRef](#)]
3. Mao, X.; Wang, Y.; Zhan, H.; Feng, L. Geochemical and isotopic characteristics of geothermal springs hosted by deep-seated faults in Dongguan Basin, Southern China. *J. Geochem. Explor.* **2015**, *158*, 112–121. [[CrossRef](#)]
4. Benavente, O.; Tassi, F.; Reich, M.; Aguilera, F.; Capecciacci, F.; Gutiérrez, F.; Vaselli, O.; Rizzo, A. Chemical and isotopic features of cold and thermal fluids discharged in the Southern Volcanic Zone between 32.5° S and 36° S, Insights into the physical and chemical processes controlling fluid geochemistry in geothermal systems of Central Chile. *Chem. Geol.* **2016**, *420*, 97–113. [[CrossRef](#)]

5. Tassi, F.; Liccioli, C.; Augusto, M.; Chiodini, G.; Vaselli, O.; Calabrese, S.; Pecoraino, G.; Tempesti, L.; Caponi, C.; Fiebig, J.; et al. The hydrothermal system of the Domuyo volcanic complex (Argentina): A conceptual model based on new geochemical and isotopic evidences. *J. Volcanol. Geotherm. Res.* **2016**, *328*, 198–209. [[CrossRef](#)]
6. Battistel, M.; Hurwitz, S.; Evans, W.C.; Barbieri, M. The chemistry and isotopic composition of waters in the low-enthalpy geothermal system of Cimino-Vico Volcanic District, Italy. *J. Volcanol. Geotherm. Res.* **2016**, *328*, 222–229. [[CrossRef](#)]
7. Luo, L.; Pang, Z.; Liu, J.; Hu, S.; Rao, S.; Li, Y.; Lu, L. Determining the recharge sources and circulation depth of thermal waters in Xianyang geothermal field in Guanzhong Basin: The controlling role of Weibei Fault. *Geothermics* **2017**, *69*, 55–64. [[CrossRef](#)]
8. Avşar, Ö.; Kurtuluş, B.; Gürsu, S.; Kuşcu, G.G.; Kaçaroğlu, F. Geochemical and isotopic characteristics of structurally controlled geothermal and mineral waters of Muğla (SW Turkey). *Geothermics* **2016**, *64*, 466–481. [[CrossRef](#)]
9. Roquer, T.; Arancibia, G.; Rowland, J.; Iturrieta, P.; Morata, D.; Cembrano, J. Fault-controlled development of shallow hydrothermal systems: Structural and mineralogical insights from the Southern Andes. *Geothermics* **2017**, *66*, 156–173. [[CrossRef](#)]
10. Zhang, Y.; Tan, H.; Zhang, W.; Wei, H.; Dong, T. Geochemical constraint on origin and evolution of solutes in geothermal springs in western Yunnan, China. *Chem. Der Erde—Geochem.* **2016**, *76*, 63–75. [[CrossRef](#)]
11. Han, D.; Liang, X.; Currell, M.J.; Song, X.F.; Chen, Z.Y.; Jin, M.G.; Liu, C.; Han, Y. Environmental isotopic and hydrochemical characteristics of groundwater systems in Daying and Qicun geothermal fields, Xinzhou Basin, Shanxi, China. *Hydrol. Process.* **2010**, *24*, 3157–3176. [[CrossRef](#)]
12. Sayres, D.S.; Pfister, L.; Hanisco, T.F.; Moyer, E.J.; Smith, J.B.; St. Clair, J.M.; O'Brien, A.S.; Witinski, M.F.; Legg, M.; Anderson, J.G. Influence of convection on the water isotopic composition of the tropical tropopause layer and tropical stratosphere. *J. Geophys. Res.* **2010**, *115*, D00J20. [[CrossRef](#)]
13. Baba, A.; Yuce, G.; Deniz, O.; Ugurluoglu, D.Y. Hydrochemical and Isotopic Composition of Tuzla Geothermal Field (Canakkale-Turkey) and its Environmental Impacts. *Environ. Forensics* **2009**, *10*, 144–161. [[CrossRef](#)]
14. Newell, D.; Crossey, L.; Karlstrom, K.; Fischer, T.; Hilton, D. Continental-scale links between the mantle and groundwater systems of the Western United States; evidence from travertine springs and regional He isotope data. *GSA Today* **2005**, *15*, 4–10. [[CrossRef](#)]
15. Guo, Q.; Wang, Y.; Liu, W. O, H, and Sr isotope evidences of mixing processes in two geothermal fluid reservoirs at Yangbajing, Tibet, China. *Environ. Earth Sci.* **2010**, *59*, 1589–1597. [[CrossRef](#)]
16. Dotsika, E.; Poutoukis, D.; Kloppmann, W.; Guerrot, C.; Voutsas, D.; Kouimtzis, T.H. The use of O, H, B, Sr and S isotopes for tracing the origin of dissolved boron in groundwater in Central Macedonia, Greece. *Appl. Geochem.* **2010**, *25*, 1783–1796. [[CrossRef](#)]
17. Pasvanoğlu, S.; Chandrasekharam, D. Hydrogeochemical and isotopic study of thermal and mineralized waters from the Nevşehir (Kozakli) area, Central Turkey. *J. Volcanol. Geotherm. Res.* **2011**, *202*, 241–250. [[CrossRef](#)]
18. Liu, K.; Qiao, X.; Li, B.; Sun, Y.; Li, Z.; Pu, C. Characteristics of deuterium excess parameters for geothermal water in Beijing. *Environ. Earth Sci.* **2016**, *75*, 1485. [[CrossRef](#)]
19. Guo, Q.; Pang, Z.; Wang, Y.; Tian, J. Fluid geochemistry and geothermometry applications of the Kangding high-temperature geothermal system in eastern Himalayas. *Appl. Geochem.* **2017**, *81*, 63–75. [[CrossRef](#)]
20. Tu, L.; Wang, H.; Feng, Y. Research on D and O<sup>18</sup> isotope in the precipitation of Guilin. *Carsol. Sin.* **2004**, *23*, 304–309.
21. Guan, H.; Simmons, C.T.; Love, A.J. Orographic controls on rain water isotope distribution in the Mount Lofty Ranges of South Australia. *J. Hydrol.* **2009**, *374*, 255–264. [[CrossRef](#)]
22. Liu, J.; Song, X.; Yuan, G.; Sun, X.; Liu, X.; Wang, S. Characteristics of  $\delta^{18}\text{O}$  in precipitation over Eastern Monsoon China and the water vapor sources. *Chin. Sci. Bull.* **2010**, *55*, 200–211. [[CrossRef](#)]
23. Parkhurst, D.L.; Appelo, C.A.J. Description of input and examples for PHREEQC version 3—A computer program for speciation, batch-reaction, one-dimensional transport, and inverse geochemical calculations. In *U.S. Geological Survey Techniques and Methods, Book 6*; 2013; Chapter A43; 497p. Available online: <http://pubs.usgs.gov/tm/06/a43> (accessed on 2 December 2016).
24. Giggenbach, W.F. Geothermal solute equilibria. Derivation of Na-K-Mg-Ca geoindicators. *Geochim. Cosmochim. Acta* **1988**, *52*, 2749–2765. [[CrossRef](#)]

25. Fournier, R.O. A Revised Equation for the Na/K Geothermometer. *Geotherm. Resour. Counc. Trans.* **1979**, *3*, 221–224.
26. Verma, M.P. Silica Solubility Geothermometers for Hydrothermal Systems. In Proceedings of the Tenth International Symposium on Water-Rock Interaction, WRI-10, Villasimius, Italy, 10–15 June 2001; Volume 1, pp. 349–352.
27. Verma, M.P.; Santoyo, E. New improved equations for Na/K, Na/Li and SiO<sub>2</sub> geothermometers by outlier detection and rejection. *J. Volcanol. Geotherm. Res.* **1997**, *79*, 9–24. [[CrossRef](#)]
28. Fournier, R.O. Chemical geothermometers and mixing models for geothermal systems. *Geothermics* **1977**, *5*, 41–50. [[CrossRef](#)]
29. Yuan, Y.; Ma, Y.; Hu, S.; Guo, T.; Fu, X. Present-Day Geothermal Characteristics in South China. *Chin. J. Geophys.* **2006**, *49*, 1005–1014. [[CrossRef](#)]



© 2019 by the authors. Licensee MDPI, Basel, Switzerland. This article is an open access article distributed under the terms and conditions of the Creative Commons Attribution (CC BY) license (<http://creativecommons.org/licenses/by/4.0/>).